Pentaquarks in QCD

Madalena Lourenço
madalena.c.lourenco@tecnico.ulisboa.pt

Instituto Superior Técnico, Lisboa, Portugal

December 2020

Abstract

For many decades after the invention of the quark model by Murray Gell-Mann and, independently, George Zweig in 1964, there was no evidence that hadrons are formed from anything other than the simplest combinations of quarks and antiquarks. In the last decade, however, in an explosion of data from hadron colliders, many recently observed states do not fit into this picture: exotic hadrons. They can be explained if the new mesons contain two quarks and two antiquarks (tetraquarks), while the baryons contain four quarks plus an antiquark (pentaquarks). The theoretical explanations for these pentaquark states take two divergent tracks: tightly bound objects, or loosely bound "molecules" formed of a meson and a baryon. The goal of this thesis project is to calculate pentaquark states in QCD within the Bethe-Salpeter formalism and make predictions for these observed LHCb states made of light and charm quarks. The main objective is to solve, numerically, a two-body equation for a meson-baryon system, which couples the relevant channels in the equation. In our approach, the interaction between the meson-baryon molecule is shaped by one-boson exchanges.

Keywords: Bethe-Salpeter equations, coupled channel equation, exotic hadrons, pentaquarks.

1. Introduction

In recent years, with an explosion of data from hadron colliders, particle physicists have seen a remarkable boost in the knowledge of baryons and mesons in the heavier sector (*1–4*), and some of these recently observed states do not fit into the quark model picture for hadrons, where mesons are made of a quark-antiquark pair, and baryons of three quarks. This leads to their categorization as exotics due to their divergent characteristics from the ordinary states. It can be assumed that lower-mass exotic mesons are constituted of four (anti-)quarks, called tetraquarks, and baryons of five (anti-)quarks named pentaquarks (*5*). Mainly, exotics are found in the charmonium regions ($c\bar{c}$), motivating the new configurations depicted in Figure 1. Recently, a new exotic particle was discovered, suggesting a $cc\overline{cc}$ composition (*6*).

Several theoretical models for exotic states have been developed and take divergent assumptions: tightly bound particles with four or five constituents, or loosely bound "molecules" like the deuteron but made of hadrons (*7*). The fact that exotic baryons also appear close to thresholds motivates a molecular picture for pentaquark states as well.

Progress in this field also ties into precision measurements of the fundamental properties of hadrons, for instance, the pion, proton, and neutron, and other simple nuclei to compare with the theoretical calculations and allow for a quantitative description of their internal structure.

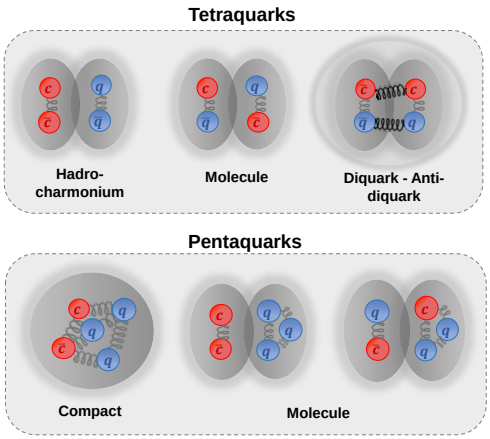

Figure 1: Schematic representation of the possible tetraquark and pentaquark configurations.

After 50 years without robust experimental candidates for pentaquarks, in 2015 a short-lived pentaquark was observed through the decay of unstable particles in the LHCb experiment at CERN (*1*), by studying the decays of $\Lambda_b^0 \to J/\psi K^- p$, particularly the spectrum of the $J/\psi p$ decay mode mass. The

LHCb collaboration established the existence of two pentaquark states constituted by $c\bar{c}uud$, making them "charmonium" pentaquarks

In 2019, combining the data from Run 1 and Run 2 and having a better resolution near the peaks, (*4*), the LHCb collaboration discovered a third pentaquark, labeled as $P_c(4312)^+$, which was observed with a statistical significance of 7.3σ. There is also 5.4σ evidence that the mass peak in the Run 1 data associated with $P_c(4450)^+$ actually consists of two peaks, which suggests that these correspond to two different pentaquarks, $P_c(4440)^+$ and $P_c(4457)^+$. In these fits, $P_c(4380)^+$ can neither be confirmed nor contradicted. The results are represented in Figure 2. The three peaks are narrow, which means that the pentaquark particles have relatively long lifetimes before they decay, suggesting that these states resemble molecules holding a baryon and a meson bound together by a residual strong force, as represented by the molecules in Figure 1.

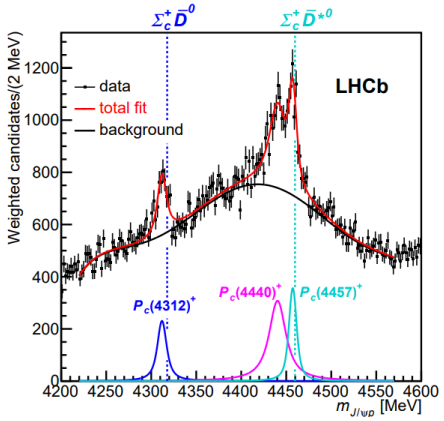

Figure 2: Fit to the weighted $m_{J/\psi p}$ distribution, which is used to determine the central values of the masses and widths of the P_c^+ states. The mass thresholds for the $\Sigma_c^+\overline{D}^0$ and $\Sigma_c^+\overline{D}^{*0}$ final states are superimposed (*4*).

2. Bound state equations

Bound states appear as poles in the n-point Green functions, which encode hadron properties. In particular, a meson corresponds to a pole in the four-point and a baryon in the six-point Green functions, $G^{(2)}$ and $G^{(3)}$, or correspondingly in the scattering matrices, $T^{(2)}$ and $T^{(3)}$. In the Euclidean metric, the total momentum at the pole $P^2 = -M^2$ corresponds to the bound state mass, M, which is determined by solving the corresponding Bethe-Salpeter Equation (BSE) (*8*, *9*).

2.1. Dyson's equations

In order to derive the BSE, the starting point is the generalized Dyson equation for the n-point Green functions $G^{(n)}$ or equivalently for the n-point scattering matrix $T^{(n)}$, given by:

$$\begin{aligned} G^{(n)} =& G_0^{(n)} + G_0^{(n)}\, K^{(n)}\, G^{(n)}\,, \\ G^{(n)} =& G_0^{(n)} + G_0^{(n)}\, T^{(n)}\, G_0^{(n)} \;\Leftrightarrow \\ \Leftrightarrow\, & T^{(n)} = K^{(n)} + K^{(n)}\, G_0^{(n)}\, T^{(n)} \end{aligned} \tag{1}$$

where $G_0^{(n)}$ is the product of n disconnected dressed quark propagators, $G^{(n)}$ is the amputated and connected part of the n-point functions, $K^{(n)}$ corresponds to the n-point scattering kernel, and $T^{(n)}$ is the connected and fully amputated scattering kernel. The last equation in (1) is depicted in Figure 3 - *left*.

Then, at the pole, the corresponding BS wave function Ψ is the residue of the Green function $G^{(n)}$ and the BS amplitude Γ is the residue of the scattering matrix $T^{(n)}$,

$$\begin{gathered} G^{(n)} \to \mathcal{N}\frac{\Psi\overline{\Psi}}{P^2 + M^2}\,, \quad T^{(n)} \to \mathcal{N}\frac{\Gamma\overline{\Gamma}}{P^2 + M^2}\,, \\ \Psi = G_0^{(n)}\Gamma\,, \end{gathered} \tag{2}$$

where P is the total momentum at the pole, and $\mathcal{N}$ is the normalization constant that depends on the spin of the resulting particle.

Inserting equation (2) into the Dyson equations (1), we identify the pole in G and T by comparing the residues on both sides of the equations that yield the homogeneous equation at the pole, either formulated in terms of the wave function Ψ or the amplitude Γ:

$$\Psi^{(n)} = G_0^{(n)} K^{(n)} \Psi^{(n)}, \quad \Gamma^{(n)} = K^{(n)} G_0^{(n)} \Gamma^{(n)}. \tag{3}$$

This is called the Bethe-Salpeter Equation. In order to solve this equation, one needs knowledge of the propagators S_i and the kernel.

For example, the Bethe-Salpeter equation for a quark-antiquark bound state is the particular case of equation (3) for $n = 2$. If we drop for now the flavor and color indices, the equation is given by:

$$\Gamma^{\mu_j}_{\alpha\beta}(p,P) = \int_q K_{\alpha\gamma,\delta\beta}(p,q,P)\big\{S(q_+)\Gamma(q,P)^{\mu_j} S(q_-)\big\}_{\gamma\delta} \tag{4}$$

where $S(q)$ is the quark propagator, whose general form is given in eq. (5). The momenta are defined as $q_+ = q + \eta P$ and $q_- = q - (1-\eta)P$, with η being the momentum-partioning. The greek letters represents the Dirac indices and μ_j the Lorentz indices. This equation is schematically represented in Figure 3 - *right*.

The most general form of a Green function follows from the Lorentz invariance, so one can expand the correlation functions in Lorentz-invariant dressing-functions and Lorentz-covariants tensors that inherit the symmetries of G:

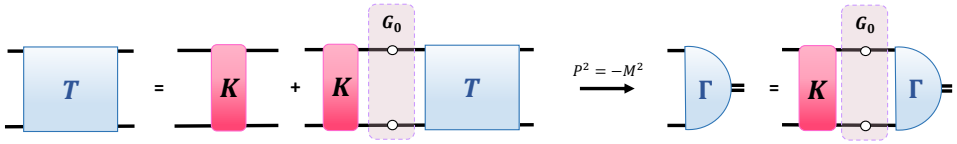

Figure 3: The Dyson equation (1) for a four-point scattering matrix (*left*). Schematic representation of the bound-state equation for the BS amplitude at the pole position (*right*).

$$G^{\mu\nu\cdots}_{\alpha\beta\cdots}(p_n) = \sum_{i=1}^{N} f_i\left(p_1^2, p_2^2, p_1\cdot p_2, \ldots\right)\tau^{\mu\nu\cdots}_{i,\alpha\beta\cdots}(p_n)\,, \quad (5)$$

where f_i are the Lorentz invariant dressing functions that only depend on invariant quantities, and τ_i are the Lorentz-covariant tensors that depend on all momentum variables.

For example, the quark propagator is deduced from the Lorentz invariance in the following way: the propagator can only depend on two Dirac structures $\{I, \not{p}\}$ since the remaining ones have wrong parity when including the γ_5 matrix. Thus, the most general structure with these tensors is given by:

$$S(p) = \frac{Z_f(p^2)}{p^2 + M(p^2)^2}(-i\not{p} + M(p^2))\,, \quad (6)$$

where $M(p^2)$ is the quark mass function and $Z_f(p^2)$ the renormalization function.

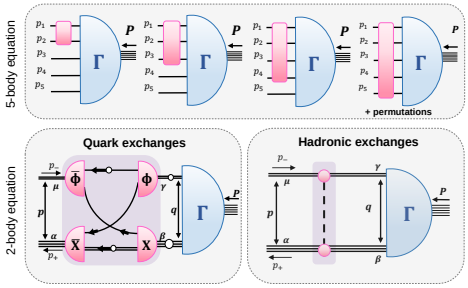

Figure 4: Schematic representation of the possible pentaquark pictures: 5-body system (*top*), and meson-baryon configurations with quark exchanges or hadronic exchanges (*bottom*). The latter is the model used in our calculations.

3. Pentaquarks

A pentaquark system constitutes a five-body problem, which is difficult to solve on technical grounds, considering the large number of independent momenta and tensor structures in the equation. However, the problem can be simplified to a two-body system where the pentaquark is described as a "molecule" made of a baryon and a meson as shown in Figure 4. A formal analogy is the reduction of the three-body problem for baryon to a quark-diquark picture, which also results in a two-body system with fermion (quark) and boson (diquark) constituents (*10*, *11*).

In the case of pentaquarks, the degrees of freedom are mesons and baryons, where hadronic exchanges give the interaction kernel.

3.1. Propagators, kernels, and vertices

The meson and baryon propagators are taken to be free propagators. The pseudoscalar-meson, vector-meson and baryon propagators are then given by

$$D_P(q) = \frac{1}{q^2 + M_P^2}\,, \quad D_V^{\mu\nu}(q) = \frac{1}{q^2 + M_V^2}\,T_q^{\mu\nu}\,, \quad S(q) = \frac{-i\not{q} + M_b^2}{q^2 + M_b^2}\,, \quad (7)$$

where q is the momentum of the particle, M is the mass, and $T_q^{\mu\nu} = \left(\delta^{\mu\nu} - \frac{q^\mu q^\nu}{q^2}\right)$ is the transverse projector.

The vertex interactions have to conserve the quantum numbers, including, for example, spin and isospin. Consequently, the particles exchanged have to be bosons to conserve spin and their quark content has to be $\bar{q}q$, with $q = u, d$ or c to conserve isospin and be color neutral. Lastly, depending on the spin of the meson that is considered in the molecule, the exchanged mesons can be scalar, pseudoscalar and vector. Each vertex has an associated coupling constant, denoted by $\alpha_i, i = 1, 2$, where 1 stands for the baryon-boson interaction and 2 for the meson-boson one. The coupling constants enter the kernel, and they measure the strength of that individual interaction. In our simple model, these couplings are assumed to be equal in all vertices. Ideally, the couplings' values could be calculated self-consistently from QCD through the construction of the relevant invariant transition matrix elements by mediating the transition between the three hadrons, for example by triangle diagrams on the vertices (*12*).

The interaction kernels are given by the product of the vertex tensors and the scalar factor $1/(k^2 + m^2)$, where k is the momentum of the exchanged particle and m its mass. The one-boson-exchange kernels are written as:

Scalar exchanges:

$$K_{PP}(k) = \frac{\alpha}{k^2 + m^2}\,, \; K_{VV}^{\mu\nu}(k) = \frac{\alpha\,\delta^{\mu\nu}}{k^2 + m^2}\,, \quad (8)$$

Vector exchanges:

$$K_{PP}(k) = \frac{i\alpha\gamma^\mu k^\mu_{rel}}{k^2+m^2}\,,\; K^\nu_{PV}(k) = \frac{\alpha\,\epsilon^{\mu\nu\delta\gamma}\gamma^\mu k^\gamma q^\delta_-}{k^2+m^2}\,, \quad (9)$$

Pseudoscalar exchanges:

$$K^\nu_{PV}(k) = \frac{\alpha\,\gamma_5 k^\nu_{rel}}{k^2+m^2}\,,\; K^{\mu\nu}_{VV}(k) = \frac{\alpha\,\epsilon^{\mu\nu\delta\gamma}\gamma_5 p^\gamma_-\, q^\delta_-}{k^2+m^2}\,, \quad (10)$$

where k_{rel} is the relative momentum between the two pseudoscalar particles. The first superscript identifies the initial meson and the second the meson after the boson being exchanged. P means pseudoscalar and V vector meson, and α corresponds to the product of the coupling constants at each vertex, $\alpha = \alpha_1\alpha_2$.

The structure of the kernels where the vector meson after the exchange is converted into a pseudoscalar meson, K_{VP}, is the same as in the K_{PV} case. The only difference is in the relative momentum, which is always defined between the two pseudoscalar particles.

3.2. Coupled channel equation

Having established all ingredients beforehand - the propagators and kernels -, we are in a position to solve the Bethe-Salpeter equation that couples all relevant channels of the system. The resulting equation has the same structure as eq. (3). In this case S is the baryon propagator and the meson propagators (D) are defined in eqs. (7). The BSE is written as

$$\Gamma^\mu_{a,\alpha\beta}(p,P) = \int_q \Big\{K^{\mu\nu}_{ab}(p,q,P)\,S_b(q_+)\times \times\,\Gamma^\gamma_b(q,P)\Big\}_{\alpha\beta} D_b{}^{\nu\gamma}(q_-)\,, \quad (11)$$

where the index a stands for the initial channel and b for the intermediate state. The indices μ,ν and γ are the Lorentz indices, where we combine pseudoscalar and vector constituents into Lorentz indices $\mu = 0\ldots4$. $p_\pm$ is the external momenta of the propagators and $q_\pm$ is the internal momenta.

3.3. Pentaquark system

We model the pentaquark by a meson-baryon molecule and include all channels that can form a $c\bar{c}uud$ content. There are two possible combinations for the initial and final states:

$$(c\bar{c}) + (qqq) \quad \text{or} \quad (\bar{c}q) + (cqq)\,,$$

where q means a light quark, u or d, which are the same since we assume isospin symmetry, and c is a charm quark. These two possibilities for the molecular configurations are given in Figure 1. For instance, a possible molecule is formed by the meson $D\,(\bar{c}q)$ and the baryon $\Sigma_c\,(cqq)$. For the exchanged particles, we consider the light mesons σ,ρ and π ($\sim\bar{q}q$), and the charmed mesons $\overline{D}$ and $\overline{D}^*\,(\bar{c}q)$.

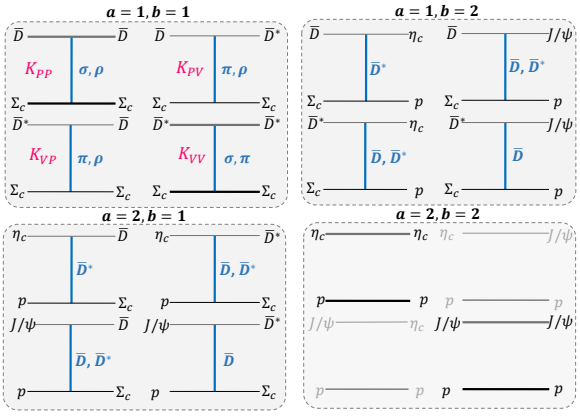

Figure 5: Possible channels and exchanged particles for the pentaquark system. Gray solid lines represent a general meson and solid black lines a fermion; the blue line is a generic interaction. Each kernel of the four channels has the structure represented in the first diagram.

The possible channels and exchanged particles are presented in Figure 5. The interactions between $\eta_c p$ and $J/\psi p\,(a=2, b=2)$ are suppressed since light quarks can only couple to c via quark-disconnected (and thus OZI-suppressed) diagrams, which is the reason why they are not considered in our calculations. However, other channels can fluctuate into these through two-loop diagrams justifying why even though the $\eta_c p$ and $J/\psi p$ thresholds are lower, they are not the dominant contributions to the pentaquark states. The $\Lambda_c\overline{D}$ system has the suitable quark content to form a pentaquark state, however it was found to be repulsive (*13*).

The natural quantum numbers for bound states made of $J^P = (1/2)^+$ baryons (Σ_c, p) and mesons with $J^P = 0^-$ $(\overline{D}, \eta_c)$ or 1^- $(\overline{D}^*, J/\psi)$ are $J^P = (1/2)^-$ and $(3/2)^-$. In the following we only consider the $(1/2)^-$ case, for simplicity.

4. Numerical techniques

We want to solve a Bethe-Salpeter equation for a two-body system with $J^P = (1/2)^-$ with a one-boson exchange. Thus, we start by working out the BSE for the first channel $(\Sigma_c\{\overline{D}, \overline{D}^*\} \leftrightarrow \Sigma_c\{\overline{D}, \overline{D}^*\})$, only. The structure of the kernels and propagators is the same for each channel; hence, in the following equations the channel indices are omitted. Furthermore, we assume that the exchanged particles have already been summed up when the coupling constant $\alpha_{ab,\text{ex}}$ is multiplied in the kernel with the factor $1/(k^2+m^2)$, which is the only quantity that depends on the exchanged particle.

To solve the BSE, the BS amplitudes (given in eq. (11)) and the wave functions defined as $\chi^{\nu}_{b,\alpha\beta}(q,P) = \left\{S_b(q_+)\,\Gamma^{\gamma}_b(q,P)\right\}_{\alpha\beta} D^{\nu\gamma}_b(q_-)$ are expanded into Lorentz scalar functions f_i and g_i, and Dirac basis elements $\tau^{\mu}_{i,\alpha\beta}$:

$$\begin{aligned}\Gamma^{\mu}_{\alpha\beta}(p,P) &= \sum_{i=1}^{8} f_i(p^2,z,P^2)\,\tau^{\mu}_{i,\alpha\beta}(p,P)\,,\\ \chi^{\mu}_{\alpha\beta}(q,P) &= \sum_{j=1}^{8} g_j(q^2,z',P^2)\,\tau^{\mu}_{j,\alpha\beta}(q,P)\,.\end{aligned} \tag{12}$$

There are eight basis elements, where the first two describe the Dirac and Lorentz structure of the pseudoscalar part and the rest the vector part. The Dirac basis elements result from a particular representation of the symmetry properties of the state under parity and spin. For numerical convenience, we use an orthonormal basis such that f_i and g_i are obtained directly by projection. The orthonormal basis elements obey the following orthonormality property: $\frac{1}{2}\mathrm{Tr}\left\{\overline{\tau}^{\mu}_i(p,P)\,\tau^{\mu}_j(p,P)\right\} = \delta_{ij}$, where $\overline{\tau}^{\mu}_i(p,P)$ is the conjugate basis element, constructed in such a way that makes the basis orthonormal. Accordingly, there are eight Lorentz scalar functions f_i and g_i that depend on all possible Lorentz invariant momentum variables and inherit the symmetries of the amplitudes and wave functions. Therefore, the quantities Γ^{μ} and χ^{μ} are completely defined by these covariants.

Then, we expand the BS amplitudes and wavefunctions in the basis $\tau_i(p,P)$ and project into $\overline{\tau}_j(p,P)$ to obtain the dressing functions of the amplitudes and the wavefunctions.

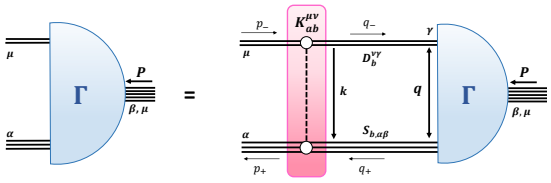

Figure 6: Pictorial representation of the BSE given in eq. (11).

The basis expansion results into an 8×8 matrix that corresponds to the distinct kernels of each channel. For instance, in Figure 5, the kernel of the $\Sigma_c\overline{D}-\Sigma_c\overline{D}$ diagram of the first channel ($a=b=1$) corresponds to K^{PP}_{ij}, where $i,j=1,2$ since the meson $\overline{D}$ is a pseudoscalar meson, while the kernel of the second diagram $\Sigma_c\overline{D}-\Sigma_c\overline{D}^*$ is K^{PV}_{ij}, where $i=1,2$; $j=3...8$ since the meson $\overline{D}^*$ is a vector.

Then, one implements the expansion and projection in eq. (12) to $\chi^{\mu}_{\alpha\beta}(q,P)$ to obtain the propagator dressing functions. In the same way as the kernel, the expansion results into an 8×8 matrix. There are no mixed propagators, so one only has the baryon by pseudoscalar-meson propagator product, given by G^{PP}_{ij}, and the product of the baryon by the vector meson, written as G^{VV}_{ij}. For instance, $\Sigma_c\overline{D}$ corresponds to G^{PP}_{ij}, where $i,j=1,2$ since $\overline{D}$ is a pseudoscalar propagator, and $\Sigma_c\overline{D}^*$ to G^{VV}_{ij}, where $i,j=3...8$ since $\overline{D}^*$ is a vector meson.

For later convenience, we expand the kernel K_{ij} and the propagator G_{ij} into Chebyshev polynomials of the second kind which hold the dependence on the angular variables z and z'. Thereafter, the full matrix is calculated by multiplying the kernel and the propagator matrices, and performing the integration over the momentum variables leads to the following equation:

$$f_{im}(p^2) = \sum_{jn} \underbrace{\int dq^2 K_{ikmr}(p^2,q^2,P^2) G_{kjrn}(q^2,P^2)}_{\mathbf{K}^{\mathcal{Q}}_{ijmn}(P^2)} f_{jn}(q^2)\,, \tag{13}$$

where $\mathbf{K}^{\mathcal{Q}}_{ijmn}(P^2)$ is the full kernel matrix that defines each channel. The index $\mathcal{Q}$ stand for the discretized momentum dependence. The dimension of the matrix $K^{\mathcal{Q},ab}_{ijmn}(P^2)$ is given by $(n_p \times n_{cheb} \times n_{ch} \times 8,\, n_p \times n_{Cheb} \times n_{ch} \times 8)$, where n_p represents the number of grid points to calculate the integration in the radial variable p, n_{Cheb} is the number of Chebyshev moments, 8 is the number of basis elements and n_{ch} is the number of channels.

Finally, having calculated the full kernel for each channel, one can sum over the indices of the final channel b, by transforming the system into a matrix-vector multiplication. An artificial eigenvalue $\lambda(P^2)$ is introduced and the eigenvectors F represent the BS amplitudes $\Gamma^{\mu}_{a,\alpha\beta}(p,P)$. The equation is

$$\lambda(P^2)\,F^a_{im} = K^{\mathcal{Q},ab}_{ijmn}(P^2)\,F^b_{jn}\,. \tag{14}$$

To find a bound state solution, we vary P^2 to identify the values where some of the eigenvalues become one, which then corresponds to the mass of a possible bound state. More efficiently, we calculate the kernel with all coupling constants equal to 1. Thus for any P^2, the inverse eigenvalues $1/\lambda(P^2)$ is a value of a common coupling constant c, by which we can multiply the kernel to produce a bound state. The smallest corresponds to a ground state's mass and the larger ones to possible excited states.

4.1. Eigenvalue reconstruction

The kernel K and the propagator G matrices are both hermitian but $(KG) \neq (KG)^{\dagger}$ because they do not commute. For unequal masses, solutions with different type of eigenvalues may interfere,

and this could be the underlying mechanism for the generation of complex eigenvalues (*14*). In principle, the kernel and the propagator matrices can always be transformed into real and symmetric matrices: $G_{mn}(p^2, P^2) = G_{nm}(p^2, P^2)$ and $K_{mn}(p^2, p'^2, P^2) = K_{nm}(p'^2, p^2, P^2)$. Initially, due to choices of particular bases and polynomials, the matrix entries can be real or imaginary, so we perform the following transformation to make K and G real and symmetric,

$$K\,G\,\Gamma_i = \lambda_i \Gamma_i \rightarrow \underbrace{(hKg)}_{\text{real and symmetric}} \underbrace{(g^\dagger G h^\dagger)}_{\text{real and symmetric}} (h\Gamma_i) = \lambda_i\,(h\Gamma_i)\,, \tag{15}$$

where g and h are diagonal matrices with entries 1 or i.

If K and G are real and symmetric, then from a Cholesky decomposition one can show that KG is hermitian if $G > 0$ or $G < 0$. So, performing a spectral decomposition of the propagator matrix from its eigenvalues η_i and eigenvectors ξ_i, we get:

$$G\,\xi_i = \eta_i \xi_i \rightarrow G' = \sum_{\eta_i > 0 \text{ or } \eta_i < 0} \eta_i\,\xi_i \xi_i^\dagger\,, \tag{16}$$

leading to a new equation with different eigenvalues λ_i':

$$K\,G'\,\Gamma_i^{'} = \lambda_i^{'}\,\Gamma_i^{'}\,. \tag{17}$$

Because $K\,G'$ is hermitian, λ_i' must be real and the Γ_i' are orthogonal.

This restriction of the propagator matrix to its positive or negative eigenvalues disentangles the complex eigenvalues of the BSE to become real and exhibit only the characteristics of physical or unphysical solutions.

4.2. Suppression form factor

In order to make the loop integrals converge, we had to include a form factor in the kernels of eqs. (8), (9) and (10), ensuring that the BS amplitudes fall off for large momenta. This factor is given by:

$$F(q^2, \Lambda^2) = \frac{\Lambda^2}{(\Lambda^2 + q^2)}\,, \quad \Lambda = 1 \text{ GeV}\,, \tag{18}$$

where Λ is the cutoff value and q is the relative internal momentum between the two constituent particles. This monopole suppression factor is also used in other models (*5*, *15*, *16*). Before introducing this factor, the amplitudes are constant even for all p^2 values.

4.3. Eigenvalues' extrapolation

To reach the physical threshold, which corresponds to the total mass of the constituent particles in the molecule, one has to determine the optimal momentum partitioning, which allows calculations up to that limit. Only when the optimal partitioning is employed the "calculable threshold" corresponds to the physical threshold.

It is straightforward to establish this parameter for the one-channel case, it is simply given by the mass of the baryon divided by the physical threshold of the molecule. Nevertheless, when there are several channels, we have to define an optimal partitioning for each channel. In our simple model, we stick with the lower threshold, which ensures that we avoid poles; thus our thresholds correspond to the sum of the masses of the lightest baryon and meson in the channels considered. For instance, when we consider all diagrams, the calculable threshold is 2.8 GeV, which coincides with the sum of the lightest baryon, proton, and the lightest meson, $\overline{D}$.

Above the threshold, one has to extrapolate the eigenvalue spectrum which is problematic for several reasons. As a simple "guesstimate", we approximate the p^2-dependence of eigenvalues by a Hermite polynomial of degree 2. Naturally, the extrapolation is only an indication of each diagram's influence and density of eigenvalues near the threshold region. The inaccuracy of this approach is due to the fact we are continuing a non-analytical function by an analytical since there is a cut opening at the threshold(s). A proper method but more involved to extrapolate the eigenvalues is described in (*17*).

5. Results

First, we consider one channel (see Figure 5), the $\Sigma_c\{\overline{D}, \overline{D}^*\} \leftrightarrow \Sigma_c\{\overline{D}, \overline{D}^*\}$. The configurations studied for this channel are given in Figure 10 in the end. The second channel is then added, the $J/\psi p \leftrightarrow \eta_c p$, to check the eigenvalues response. The cases, including the second channel, are indicated in Figure 11. Eigenvalue comparison will allow for the assessment of their influence in the pentaquark system and determine how each channel and exchange particles affect the number of bound states.

5.1. Eigenvalue spectrum

We begin by adding diagrams to the first channel $\Sigma_c\{\overline{D}, \overline{D}^*\} \leftrightarrow \Sigma_c\{\overline{D}, \overline{D}^*\}$, as indicated by configurations **(C1) - (C4)** in Figure 10. The eigenvalue spectrum for different combinations is depicted in Figure 7.

In Figure 7 - **(C1)** and **(C2)**, we plot the inverse eigenvalue spectrum for the diagonal diagrams, individually, and looking at these configurations in Figure 10, we expect these diagrams to be decoupled, since they belong to the diagonal part of the kernel matrix. Hence, comparing the inverse eigenvalue spectrum of **(C1)** and **(C2)** with configuration **(C3)**, which includes both diagonals, we conclude that the ground and first excited state in **(C3)** are identified as the ground state in **(C1)** and the

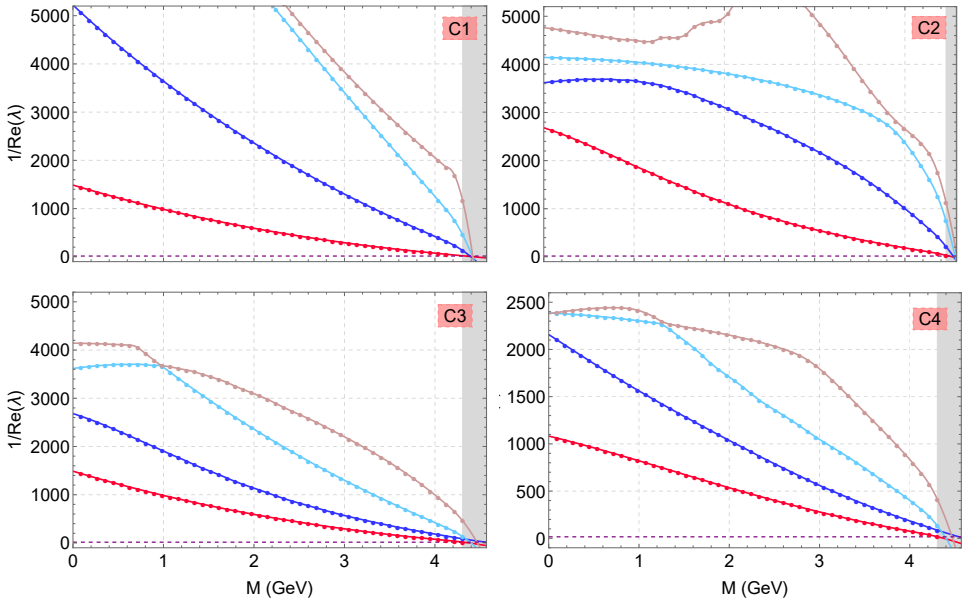

Figure 7: Inverse eigenvalue spectrum for the configurations **(C1) - (C4)** i in Figure 10 considered for the 1^{st} channel. The gray area represents the region above the threshold where the eigenvalues are extrapolated. The dots are the calculated values, the lines are inter- and extrapolation.

ground state in **(C2)**, respectively. The second and third excited states in **(C3)** have contributions from both diagrams. In particular, the second excited state is given by the first excited state in **(C2)** until around M=1 GeV and after that by the first excited state in **(C1)**. Regarding the third excited state, it is the other way around, it is dominated by the second excited state from **(C2)** until M=1 GeV and then by **(C1)**. Because the spectrum in **(C3)** can be approximately obtained by superimposing spectra **(C1)** and **(C2)**, one can conclude that these two diagrams are essentially decoupled.

Afterwards, the off-diagonal diagrams **(C4)** are included. From their comparison with **(C3)**, we observe that the spectrum is similar, but the inverse eigenvalues' magnitude in **(C4)** is lower, indicating that the off-diagonal diagrams have an attractive effect in the system; however they are not dominant.

To summarize, the first channel is essentially dominated by the diagonal diagrams, namely, in the ground state the $\Sigma_c\overline{D} - \Sigma_c\overline{D}$ diagram prevails, the first excited state is dominated by $\Sigma_c\overline{D}^* - \Sigma_c\overline{D}^*$ and the higher lying inverse eigenvalues are given by contributions from both diagonal diagrams. From now on, configuration **(C4)** will be taken as our reference.

Beyond the 1^{st} channel, we add the 2^{nd} according to configurations **(C7) - (C10)** in Figure 11, and represent the inverse eigenvalue spectrum in Figure 8.

We plot the inverse eigenvalue spectrum for **(C7)**, and comparing with our reference **(C4)** (represented by the dashed lines in all panels), one concludes that it merely shifts the spectrum. In addition, we only consider the vector-vector diagonal diagram, **(C8)** and the spectrum is almost identical to **(C7)**, but in this case the ground state is very close to our reference, meaning that the small shift from the diagonal diagrams comes from $\Sigma_c D \leftrightarrow p\,\eta_c$. Subsequently, we plot **(C9)**, and it looks very similar to the other spectra even in form and magnitude, indicating that there is not any particular diagram which is dominant. Also, we observe that the ground state is almost not changed by any of the diagrams of the 2^{nd} channel.

Finally, we plot **(C10)**, which includes all diagrams, and by comparing with **(C4)** we observe, once more, that the spectrum looks very similar. The main difference is on the inverse eigenvalues spectrum magnitude which is lowered by the interference from the diagonal and off-diagonal diagrams of the 2^{nd} channel, since the individual configurations **(C7)-(C9)** fail in explaining the **(C12)** spectrum. Despite the second channel having an attractive effect, providing more binding, it does not modify the eigenvalues fundamentally. Thus, the system is still dominated by the first channel, mainly by the diagonal diagrams.

5.2. Mass spectra

In this section, we present the mass spectra for some configurations in the first channel. The masses of the bound states $P^2 = -M^2$ are obtained by the intersection of the inverse eigenvalues with the coupling constant value. In our case, the coupling constant is chosen such that the ground state repro-

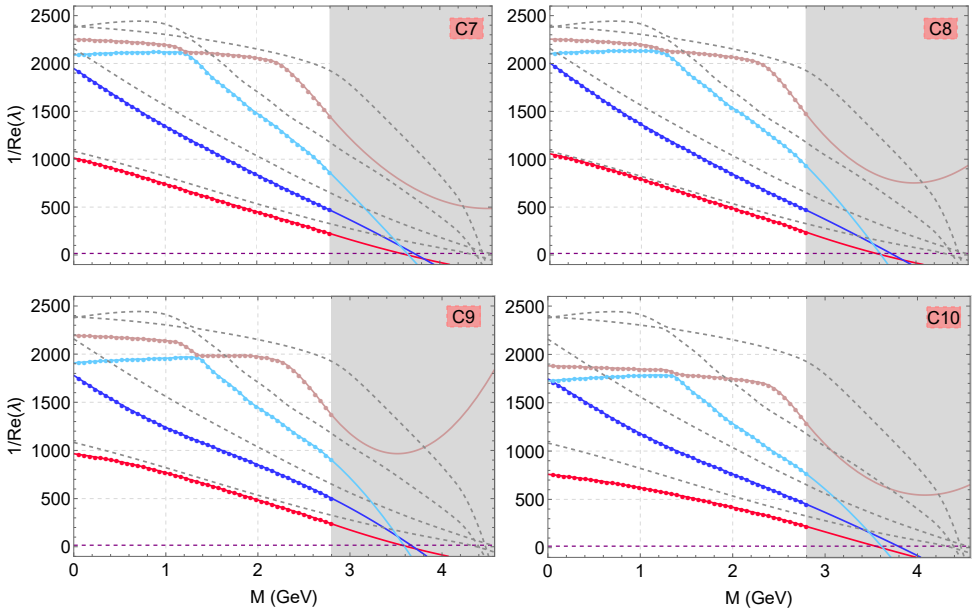

Figure 8: Inverse eigenvalue spectrum for configurations **(C7) - (C12)** in Figure 10 considered for the 1^{st} and 2^{nd} channel. The gray area represents the region above the threshold. The dashed gray lines are the results of the reference configurations **(C4)**, shown for comparison.

duces the mass of the lightest pentaquark state detected at LHC, the $P_c(4312)^+$, in our reference calculation **(C4)**. This value was found to be $c = 16.0$, which is employed in the other configurations to determine the density of bound states. As previously mentioned, this is simply a first approximation, since, in principle, one could calculate the coupling constants. Once more, the masses determined in this section are merely a rough indication, whenever they are calculated above the threshold. An evidence of the fragility of Hermite extrapolation is the occurrence of eigenvalue crossing in this region, which should not happen after the reconstruction procedure. We calculate the extrapolation until 4.457 GeV, which corresponds to the pentaquark state with the largest mass, $P_c(4457)^+$. We only consider the first three eigenvalues as an illustration. Also, higher magnitude eigenvalues are associated with larger uncertainties.

In Figure 9, the purple horizontal line is adjusted such that the first bound state in **(C4)** is at 4.312 GeV. As previously determined, the ground state in configuration **(C1)** gives the ground state in **(C4)**, so the mass of that state is the same in both cases (M = 4.312 GeV). In the first excited state, on the other hand the contribution from the ground state in **(C2)** prevails, thus the mass of the next bound state in **(C4)** should appear near 4.492 GeV. However, the second excited state in **(C4)** forms a bound state before the first excited state, as a consequence of our oversimplified extrapolation. So, if we overlook this "problematic" state, the first excited state in **(C4)** forms a bound state near 4.545 GeV, relatively close to the mass formed by the ground state in **(C2)** (M = 4.492 GeV), as one expected.

6. Conclusions

The goal of this thesis project was to calculate pentaquark states in QCD within the Bethe-Salpeter formalism. The main objective was to make predictions about the dominant diagrams to describe these states and their bound state masses. In our calculations, we assumed a molecular picture, constituted by a meson and a baryon suitable to form the appropriate quark content, $\bar{c}cuud$. Hadronic exchanges bind the molecule.

In order to draw conclusions, we plotted the inverse eigenvalue spectrum for different configurations, including the two possible channels, the $\Sigma_c\{\overline{D}, \overline{D}^*\} \leftrightarrow \Sigma_c\{\overline{D}, \overline{D}^*\}$ and the $p\{\eta_c, J/\psi\} \leftrightarrow p\{\eta_c, J/\psi\}$. Then, by comparing each channel's influence in the spectrum, we concluded that the second channel does not affect it fundamentally. It only decreases the inverse eigenvalues by providing more binding to the system. Thus, the pentaquark could be generally described by the first channel alone, as long as the molecules $\Sigma_c\overline{D}$ and $\Sigma_c\overline{D}^*$ are included. Inside the first channel, the diagonal diagrams are the most relevant to describe the system, so the case where both diagrams are included was taken as our reference case.

Afterwards, we calculated the bound state masses formed for the several combinations by fixing the coupling constant such that the first bound state in our reference case appears at the mass of the lightest

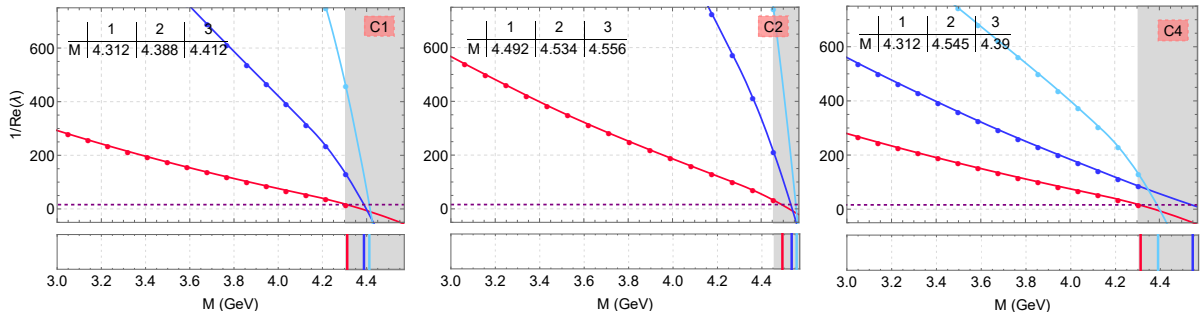

Figure 9: Inverse eigenvalue spectrum near the threshold and bound state masses for configurations **(C1), (C2)** and **(C4)**. The horizontal line corresponds to the adjusted coupling constant value, $c = 16.0$. The gray area represents the region above the threshold, where the eigenvalues are extrapolated. In the inset tables are indicated the bound state masses (in GeV) for the three eigenvalues.

pentaquark discovered at LHCb, $P_c(4312)^+$. This value was found to be $c = 16.0$. In our reference case, for the ground and first excited state, we found M = 4.312 and 4.545 GeV, respectively.

Our model is simply a first approximation; all coupling constants were taken to be equal; however, this is not a very realistic model. Each diagram has a specific coupling constant, that could be adequately calculated in future work. Another source of uncertainty is the inverse eigenvalue extrapolation above the threshold, where the masses are calculated. In principle, the predictions in this region can be made through the Resonances-Via-Padé method. Thus, our bound state masses are only an indication of the density of inverse eigenvalues near the threshold region, and should not be taken as a firm prediction.

Acknowledgements

I would like to thank my supervisors, Gernot Eichmann and Alfred Stadler.

References

1. R. Aaij *et al.*, *Phys. Rev. Lett.* **115**, 072001 (2015).
2. R. Aaij *et al.*, *Phys. Rev. Lett.* **117**, 082003 (2016).
3. S. L. Olsen, T. Skwarnicki, D. Zieminska, *Reviews of Modern Physics* **90** (2018).
4. R. Aaij *et al.*, *Phys. Rev. Lett.* **122**, 222001 (2019).
5. Y.-R. Liu, H.-X. Chen, W. Chen, X. Liu, S.-L. Zhu, **107**, 237 (2019).
6. R. Aaij *et al.*, *Science Bulletin* **65**, 1983 (2020).
7. A. Ali, J. S. Lange, S. Stone, *Prog. Part. Nucl. Phys.* **97**, 123 (2017).
8. M. Blank, A. Krassnigg, *Comp. Phys. Com.* **182**, 1391 (2011).
9. C. D. Roberts, A. G. Williams, *Prog. Part. Nucl. Phys.* **33**, 477 (1994).
10. A. Buck, R. Alkofer, H. Reinhardt, *Phys. Lett. B* **286**, 29 (1992).
11. G. Eichmann, H. Sanchis-Alepuz, R. Williams, R. Alkofer, C. S. Fischer, *Prog. Part. Nucl. Phys.* **91**, 1 (2016).
12. V. Mader, G. Eichmann, M. Blank, A. Krassnigg, *Phys. Rev. D* **84**, 034012 (2011).
13. Z.-C. Yang, Z.-F. Sun, J. He, X. Liu, S.-L. Zhu, *Chin. Phys. C* **36**, 6 (2012).
14. G. Eichmann, *Few-Body Syst.* **58**, 81 (2017).
15. R. Chen, X. Liu, S.-L. Zhu, *Nuc. Phys A* **954**, 406 (2016).
16. J. He, *Eur. Phys. Jour. C* **79**, 1 (2019).
17. G. Eichmann, P. Duarte, M. T. Peña, A. Stadler, *Phys. Rev. D* **100** (2019).

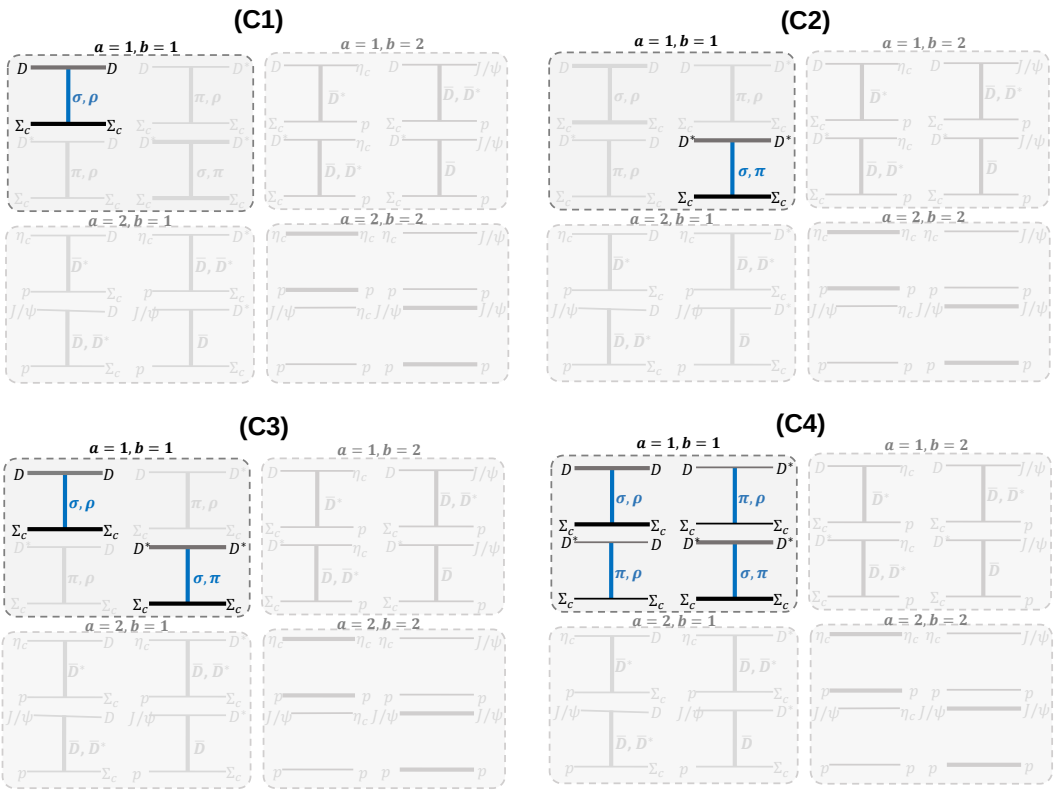

Figure 10: Different configurations considered for the first channel.

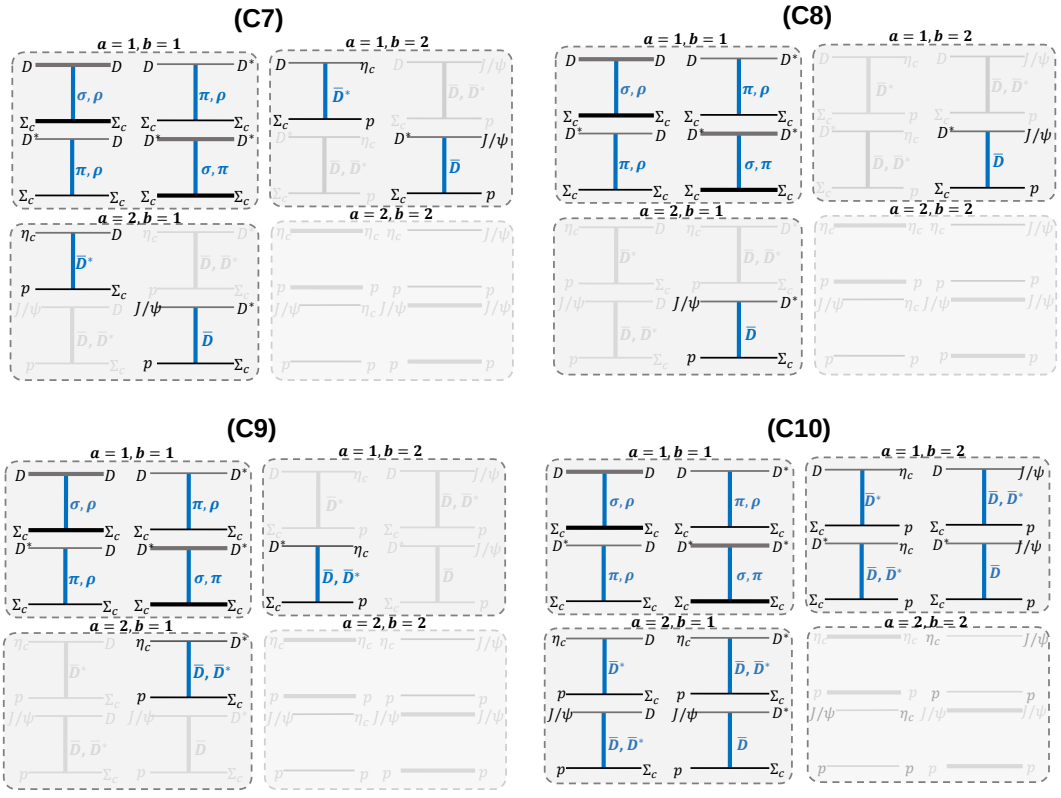

Figure 11: Different configurations considered after adding the second first channel.